Electronic Supplementary Material (ESI) for Biomaterials Science.
This journal is © The Royal Society of Chemistry 2021

Supporting Information

Visualization of USPIO-Labeled Melt-Electrowritten Scaffolds by Non-Invasive Magnetic Resonance Imaging

Kilian M. A. Mueller, Geoffrey J. Topping, Sebastian P. Schwaminger, Zou Younzhe, Diana M. Rojas-González, Elena M. De-Juan-Pardo, Sonja Berensmeier, Franz Schilling, Petra Mela

1. Materials and Methods

1. 1. Synthesis of PCL-USPIO Composites

Medical grade PCL (Purasorb PC 12, Corbion) was used as received. USPIOs were synthesized as we reported previously[1] (therein called bare iron oxide nanoparticles) with maximum size around 10 nm. Briefly: 35.0 g of iron (II) chloride and 86.4 g of iron (III) chloride, obtained from Sigma-Aldrich, were dissolved and mixed in 200 mL of deionized water. 1 M NaOH (Fluka) was prepared with deionized water and placed in a stirred tank glass reactor under a nitrogen atmosphere. Subsequently, the salt solution was added dropwise, which immediately formed a black precipitate. After complete addition, the reaction was continued for half an hour under constant conditions. The resulting particles were washed several times with deionized water until a conductivity of less than 200 µS/cm was reached. The particles were lyophilized in a freeze-drier Alpha 1-2 LDplus (Martin Christ Gefriertrocknungsmaschinen GmbH) and stored for further use. The Raman spectrum of the USPIO as produced is shown in Fig. S1.

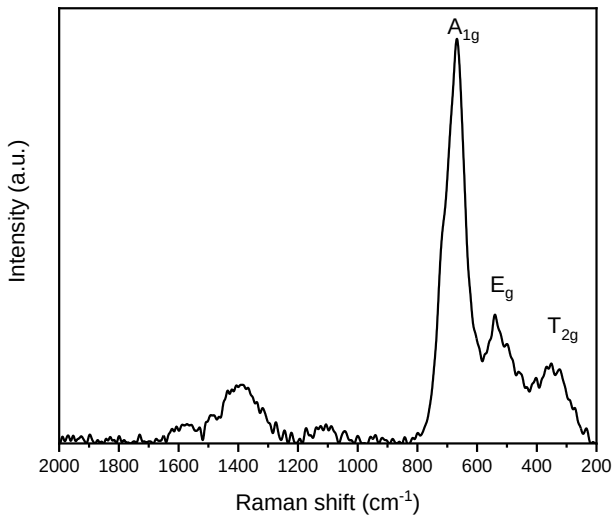

Figure S1: Raman spectrum of the synthesized USPIOs. (Reprinted with permission: S. Schwaminger, K. Schwarzenberger, J. Gatzemeier et al.: Magnetically Induced Aggregation of Iron Oxide Nanoparticles for Carrier Flotation Strategies. ACS Appl. Mater. Interfaces 2021, 13, 17, 20830-20844. Copyright (2021) American Chemical Society).

Three composites containing different weight percentages of USPIO/PCL (0.1 % w/w, 0.2 % w/w, 0.3 % w/w) were produced by dissolving 2 mg, 4 mg, and 6 mg, respectively, of USPIOs in 5 ml acetone. After 4 h sonication, homogeneous slurries without USPIO agglomerates were obtained, to each of which 2 g of PCL was added, followed by another 1 h sonication. To completely evaporate the acetone, the solutions were poured into syringes (3 cc, Nordson EFD, USA) and placed at room temperature for 48 h. In this manner, solid PCL–USPIO composites were obtained for MEW and stored at -20 °C until use. Flakes of PCL-USPIO composites were analyzed with Raman spectroscopy with a Senterra Spectrometer (488 nm laser, Bruker Optics, Germany).

1. 2. Melt-Electrowriting

PCL-USPIO composites and PCL pellets were melted in the print head at 75 °C and extruded through a 23 G needle heated to 85 °C onto a grounded flat metal collector covered by a 1 mm thick glass slide, using a previously described MEW setup.[2] Extrusion was guided with pressurized air at 2 bar applied to the syringe and a voltage of +5 kV applied to the needle. The distance between needle tip and glass slide was initially set to 3.1 mm and increased by 0.16 mm after every second layer. The relative speed between print head and laterally-moving collector was set to 360 mm/min.

For tensile testing, a series of straight lines of 40 layers was fabricated via MEW. For cytotoxicity assessment as well as MRI, a curvilinear mesh pattern of 10 layers was fabricated, as previously proposed for cardiovascular tissue engineering scaffolds.[2]

1. 3. Composites and Scaffold Analysis

Structural gross appearance of MEW scaffolds was investigated on gold sputtered scaffolds by scanning electron microscopy (accelerating voltage 10 kV, JSM-6390, Jeol). Fiber diameter was measured on 10 fibers of 3 scaffolds per composite with the SEM's built-in software.

Tensile testing was performed on a zwickiLine Z2.5 (ZwickRoell) equipped with a 10 N load cell with a crosshead speed of 10 mm/min. Each specimen (n = 10) had an initial length of 16 mm. Young's modulus was calculated between 1 % and 3.5 % strain, prior to onset of plastic deformation, and the ultimate tensile strength (UTS) was determined by the maximum stress before sample fracture.

Cytocompatibility was assessed according to IS0-10993. Melt-electrowritten squared samples (5 mm x 5 mm) were sterilized by washing them twice in 70% ethanol for 60 min each and subsequently rinsed with phosphate buffered saline (PBS). The samples were then individually placed in the wells of 96-well plate, previously seeded with human umbilical artery smooth muscle cells (HUASMCs) at a density of 10.000 cells/cm^2. Each well contained 100 µl of culture media consisting of Dulbecco's Modified Eagle's Medium (DMEM, Gibco)

supplemented with 10% fetal calf serum (FCS, Gibco) and 1% antibiotics/antimycotics (ABM, Gibco). Cell viability was assessed 1 and 3 days (n = 5 per sample group and time point) after seeding using a commercial proliferation test (XTT, Roche) and measuring optical density at 450 nm on a microplate reader (Spark, Tecan). The absorbance was normalized per day to that of the negative control. A latex glove was used as positive control. For negative control, cells were cultured in untreated medium. To check cell adherence to the materials, HUASMCs were seeded directly onto the different scaffolds and cultivated for 72 h. For evaluation, immunostaining using fluorescent phalloidin (Acti-Stain 488, Cytosceleton Inc.) and nuclei counterstaining with DAPI (Carl Roth) was performed. Samples were visualized using a fluorescence microscope (BZ-X810, Keyence).

1. 4. Magnetic Resonance Imaging

The PCL scaffold samples were embedded in 1% w/w agar-agar to assess their visibility in MRI within surrounding material. MRI was acquired with a 7 T preclinical scanner (Agilent Discovery MR901 magnet and gradient system, Bruker AVANCE III HD electronics) and a 10 mm inner diameter solenoid radiofrequency (RF) coil (RAPID Biomedical). Several image contrasts were acquired, with 0.2 mm thick slices prescribed parallel to each scaffold:

1. Nominally T1-weighted images, using a gradient recalled echo (GRE or FLASH) sequence with a single echo per RF excitation, echo time 2.57 ms, repetition time 160 ms, flip angle 10°, and 0.125x0.125 mm^2 pixels.

2. R2* maps, with a series of differently R2*-weighted images, using a multi-gradient-echo (MGE) pulse sequence with 16 echoes per RF excitation with minimum echo time 1.75 ms and echo spacing 1.09 ms, repetition time 600 ms, flip angle 30°, 0.25x0.25 mm^2 pixels, and 12 averages.

3. R2 maps, with a fast spin echo (FSE or RARE) pulse sequence with 8 echoes per excitation with minimum echo time 8 ms and echo spacing of 8 ms, separate images reconstructed for each effective echo time, repetition time 2000 ms, flip angles 90° for excitation and 180° for refocusing, 0.125x0.125 mm^2 pixels, and 4 averages.

4. R1 maps, with an inversion recovery fast spin echo (IR-FSE or IR-RARE) pulse sequence, with an adiabatic inversion preparation with 13 inversion recovery times of ranging from 10 to 5000 ms between the inversion and excitation pulses, 4 echoes per excitation, effective echo time 7.58 ms, variable repetition time but constant recovery time before inversions 2000 ms, flip angles 90° for excitation and 180° for refocusing, and 0.125x0.125 mm^2 pixels.

As detailed in the supplementary information (S.2), the relaxation rate map data was fit in each voxel independently for R1, R2, and R2*. Regions of interest (ROIs) were drawn on the

scaffolds and the R2* map signal was averaged with them, which was then fit to determine representative R2* rates for each scaffold.

1. 5. Statistical Analysis

Results are presented as mean ± standard deviation. One-way ANOVA and Dunnett's post-hoc test were performed in Prism 8 (GraphPad) after confirming normal distribution. ***: $p < 0.001$, **: $0.001 \leq p < 0.01$, and *: $0.01 \leq p < 0.05$ were used to indicate the level of significance.

2. Relaxation Rate Fitting

Reconstructed MR image data was loaded using the *pvtools* package (Bruker) and fit for relaxation rates and maps using custom-written scripts in MATLAB 2020a (The Mathworks). R2 and R2* were fit to magnitude data, while R1 was fit to complex-valued image reconstructions to retain phase information through the signal inversion and to eliminate bias from noise in magnitude data near the inversion signal null.

The longitudinal relaxation rate R1 maps were fit with a scaled-exponential plus constant model:

$$Signal(TI) = Ae^{-TI \times R1} + C$$

and the transverse relaxation rate R2 and R2* maps were fit with a scaled-exponential model:

$$Signal(TE) = Ae^{-TE \times R2(*)}$$

where TI is the inversion time (between inversion and excitation) and TE is the (effective) echo time. The scaling factor A accounts for signal variations unrelated to changes in relaxation rate, such as local proton density, radiofrequency coil sensitivity and excitation strength, and sequence timing details. The offset C accounts for background signal, such as from noise in magnitude images, which do not depend on the TE, TI, or relaxation rates, as well as the fully recovered / equilibrium magnetization signal level in the inversion recovery experiment.

Apparent average R2* rates within the scaffolds were calculated by first averaging within regions of interest (ROIs) drawn on scaffolds, and then fitting. The ROI-averaged signal was fit for R2* with an exponential plus constant model, as the simple exponential model did not fit the signal dependence well (see Figure S2). This may be in part due to the ROI-averaged signal including a mixture of different R2* components, as well as a noise floor in the data.

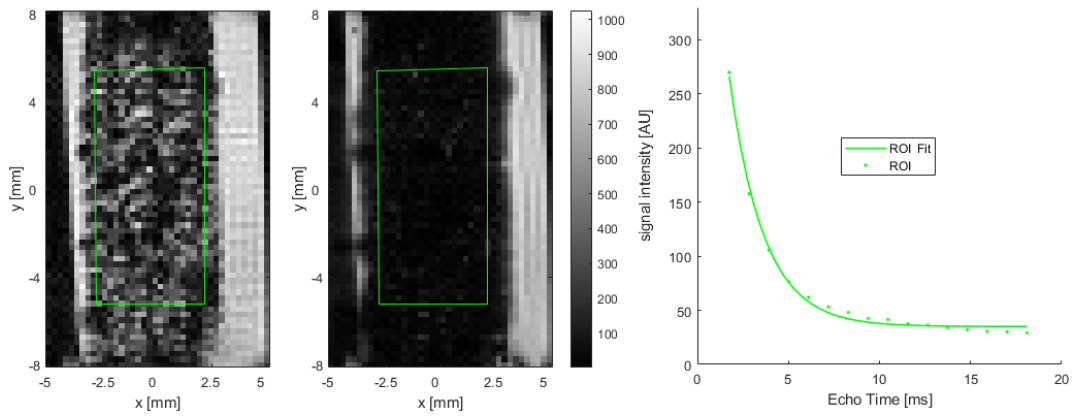

Figure S2: Multi-gradient echo (MGE) images at TE 1.75 ms (left) and 9.38 ms (middle) showing reduction in signal due to R2* being higher near the PCL scaffolds containing 0.2% w/w USPIOs. Scaled-exponential plus constant offset model curve fit (right) to ROI-averaged signals against echo time, within green outline ROI shown in the images.

3. Relaxation Measurement Discussion

The apparent relaxation rates (R1, R2, R2*) determined in this work depend on many details of the experimental setup, and will not be readily reproducible in other setups. Most clinical scanners have lower magnetic field strengths (eg. 1.5 or 3.0 T), which can affect the relaxation rates of materials (eg. agar-agar) and the relaxivity of contrast agents such as USPIOs. Different scanners also have different achievable resolutions, and lower fields also have different patterns of susceptibility artifacts around locally high accumulations of USPIOs, which may affect the resolvability of PCL scaffolds. As well, for practical biomedical applications, PCL scaffolds would likely be placed in or near tissues of substantially more complicated structure and varied R2* than uniform agar-agar gel. Depending on the inherent relaxation properties of such tissue, the amount of contrast generated by the presence of USPIO-doped scaffolds may be less than seen here.

The R2* model fit here includes a background signal term, to account for noise background in magnitude images. Without this term, a simple single exponential model would fit the relaxation curves acquired here quite poorly, and the resulting fit R2* would be severely biased to lower values by the high signal intensities at longer TE. In a lower-noise measurement, this term may not be necessary. These considerations should not alter the primary result that the addition of USPIOs to the PCL scaffolds strongly increases the MRI R2* in tissue-like material and produces strong contrast with the surroundings.

References

(1) Thomas, J. A.; Schnell, F.; Kaveh-Baghbaderani, Y.; Berensmeier, S.; Schwaminger, S. P. Immunomagnetic Separation of Microorganisms With Iron Oxide Nanoparticles. *Chemosensors* **2020**, *8* (1), 17.

(2) Saidy, N. T.; Wolf, F.; Bas, O.; Keijdener, H.; Hutmacher, D. W.; Mela, P.; De-Juan-Pardo, E. M. Biologically Inspired Scaffolds for Heart Valve Tissue Engineering via Melt Electrowriting. *Small* **2019**, *15* (24), 1900873.